Efficient reduction of Cr(VI) under visible light irradiation using CuS nanostructures

Sawsen Nezar, Yacine Cherifi, Alexandre Barras, Ahmed Addad, El Hadj Dogheche, Nadia Saoula, Nadia Laoufi, Pascal Roussel, Sabine Szunerits, Rabah Boukherroub

Arabian Journal of Chemistry (2019) **12**, 215–224

King Saud University

Arabian Journal of Chemistry

www.ksu.edu.sa
www.sciencedirect.com

ORIGINAL ARTICLE

Efficient reduction of Cr(VI) under visible light irradiation using CuS nanostructures

Sawsen Nezar [a,b,c], Yacine Cherifi [a,d], Alexandre Barras [a], Ahmed Addad [e], Elhadj Dogheche [a], Nadia Saoula [c], Nadia Aïcha Laoufi [b], Pascal Roussel [f], Sabine Szunerits [a], Rabah Boukherroub [a,*]

[a] *Univ. Lille, CNRS, Centrale Lille, ISEN, Univ. Valenciennes, UMR 8520 – IEMN, F-59000 Lille, France*
[b] *Laboratoire des phénomènes de transfert, génie chimique, Faculté de Génie des Procédés, USTHB, BP 32 El-alia, Bab Ezzouar, Alger, Algeria*
[c] *Equipe Plasma & Applications – Division des Milieux Ionisés et Lasers- Centre de Développement des Technologies Avancées – Cité du 20 Aout 1956, Baba Hassen, Alger, Algeria*
[d] *Laboratoire de Chimie Appliquée et Génie Chimique de l'Université Mouloud Mammeri de Tizi-Ouzou, Algeria*
[e] *Univ. Lille, CNRS, INRA, ENSCL, UMR 8207 - UMET - Unité Matériaux et Transformations, F-59000 Lille, France*
[f] *Univ. Lille, CNRS, ENSCL, Centrale Lille, Univ. Artois, UMR 8181 - UCCS - Unité de Catalyse et de Chimie du Solide, F-59000 Lille, France*

Received 28 August 2017; accepted 7 January 2018
Available online 17 January 2018

KEYWORDS

CuS nanostructures;
Cr(VI);
Photoreduction;
Visible light;
Lake water

Abstract Photoreduction of hexavalent chromium, Cr(VI), identified as carcinogenic and mutagenic element, to Cr(III), believed to be an essential element, using copper sulfide nanostructures (CuS NSs) as photocatalyst was investigated under visible light irradiation ($\lambda > 420$ nm). The CuS NSs were synthesized at low temperature using a wet chemical route and fully characterized using various techniques such as scanning electron microscopy, transmission electron microscopy, X-ray diffraction, X-ray photoelectron spectroscopy, Raman spectroscopy and UV–vis spectrophotometry. The photocatalytic reduction of Cr(VI) using visible light irradiation was assessed by UV–vis by following the decrease of the characteristic absorbance at ~352 nm in the presence of CuS NSs. While CuS NSs promoted Cr(VI) full reduction within 60 min, addition of adipic acid or formic acid accelerated significantly the photocatalytic reduction process. Under optimized conditions, CuS NSs rapidly (12 min) reduced Cr(VI) in presence of 0.5 mM adipic acid. Similarly, Cu NSs were found to be efficient for Cr(VI) reduction dissolved in water from a local lake. Stability studies

* Corresponding author.
E-mail address: rabah.boukherroub@univ-lille1.fr (R. Boukherroub).
Peer review under responsibility of King Saud University.

Production and hosting by Elsevier

https://doi.org/10.1016/j.arabjc.2018.01.002

showed that the photocatalyst could be recycled up to four times without any apparent decrease of its catalytic performance.

1. Introduction

Cr(VI) is widely used in industrial activities such as mining, metal plating, leather tanning, stain steel welding, water cooling, and power generation facilities. Waste streams from these industrial sites contain often Cr ions among other metal ions at concentrations above local discharge limits, and groundwater around these sites is frequently contaminated by these metal ions. However, Cr(VI) is shown to be toxic, mutagenic, and carcinogenic to humans. Indeed, several studies have demonstrated that Cr(VI) is carcinogenic to humans (Voitkun et al., 1998) and genotoxic even at non-cytotoxic concentrations (Depault et al., 2006).

To meet environmental regulations, effluents or water contaminated with Cr(VI) must be treated before discharge. Various chemical and physical techniques such as chemical precipitation, electrochemical means, mechanical filtration, ion exchange, membrane filtration, and adsorption are among the conventional methods commonly used for removal of Cr (VI) from the waste streams (Barrera-Díaz et al., 2012, Jin et al., 2016, Owlad et al., 2009, Sen and Ghosh Dastidar, 2010, Wang and Ren, 2014, Wang et al., 2017a, 2017b, Wen et al., 2016, 2017).

The Cr water solubility and its toxicity are directly related to its oxidation degree even though Cr(VI) and Cr(III) are the most stable ions found in the environment. While Cr(VI) is highly soluble in water and toxic, Cr(III) is much less soluble in water and precipitates in form of hydroxides in absence of complexing ligands. Moreover, Cr(III) is an important element for living organisms to function properly. Therefore, Cr(VI) transformation to Cr(III) under controlled conditions is an appealing method to remediate Cr(VI) contamination.

Cr(VI) chemical reduction to Cr(III) followed by precipitation is the common method to remediate wastewaters contaminated with Cr(VI). Reduced iron and reduced sulfur compounds are the common reducing agents for this transformation (Gheju, 2011). However, such processes generate large amounts of residual sludge, which are difficult in managing and final disposal as well as associated costs (Barrera-Díaz et al., 2012). Organic acids are also able to promote Cr(VI) reduction (Deng and Stone, 1996). Moreover, combined with metal nanoparticles, formic acid exhibits high efficiency for Cr(VI) reduction. Unlike other monocarboxylic acids, formic acid in the presence of palladium nanoparticles is fully mineralized to CO_2 and H_2, and the liberated H_2 is able to reduce Cr (VI) with faster rates (Celebi et al., 2016, Dandapat et al., 2011, Omole et al., 2007). More recently, the combination of organic acids and photocatalysis was successfully applied for efficient Cr(VI) reduction (Fellahi et al., 2016, Marinho et al., 2016).

The present study is focused on the performance of a new visible light active photocatalyst, copper sulfide nanostructures (CuS NSs), for the effective Cr(VI) photocatalytic reduction to Cr(III) and the influence of organic acids on the reaction kinetics.

Indeed, semiconductor chalcogenide nanostructures have generated huge interest owing to their exceptional optical and electronic properties, and their potential applications in different fields, including energy conversion devices, photocatalysis, photovoltaics, biosensors, etc... Of particular interest, copper chalcogenides, e.g. copper sulfide (CuS) represents an interesting class of materials because of its low toxicity, low cost, a wide range compositions and crystal structures, and diverse applications in various fields (Goel et al., 2014, Van Der Stam et al., 2016, Zhao and Burda, 2012). The narrow band gap (1.2–2.2 eV), which is dependent on the CuS crystalline phase, permits to harvest efficiently photons in the visible absorption window and thus makes it an interesting semiconductor for photocatalytic processes. The visible or solar light photocatalytic performance of CuS nanostructures has been evaluated for several organic pollutants such as rhodamine B (Estrada et al., 2016, Hai et al., 2013, Srinivas et al., 2015), methylene blue (Gupta et al., 2012, Hu et al., 2016, Pal et al., 2015), 2,4-dichlorophenol (Meng et al., 2013), nitrobenzene and nitrophenol (Saranya et al., 2015). Even though the photocatalytic properties of CuS nanostructures have been examined for various organic pollutants, to the best of our knowledge, the performance of this semiconductor for Cr(VI) photo-reduction has not been yet investigated.

In this paper, we studied the visible light photocatalytic performance of CuS nanostructures for Cr(VI) reduction to Cr (III) in Milli-Q or simulated water. The influence of organic acids such as formic acid or adipic acid on the degradation rate was also evaluated. The results clearly showed enhanced photocatalytic performance of the CuS NSs in presence of organic acids. In addition to the high photocatalytic activity, the CuS NSs photocatalyst exhibited good stability after several runs, which makes it reusable for this catalytic transformation.

2. Experimental part

2.1. Materials and methods

All chemicals and reagents were of analytical grade and used without any purification. Copper(II) chloride ($CuCl_2$), copper(II) sulfate pentahydrate ($CuSO_4{\cdot}5H_2O$), triethanolamine (TEA), ammonium hydroxide (NH_4OH, 28–30%), sodium hydroxide (NaOH), sodium thiosulfate (NaS_2O_3), thiourea, potassium dichromate ($K_2Cr_2O_7$), ethanol, formic acid, and adipic acid were obtained from Sigma-Aldrich (France).

A stock solution of Cr(VI) (10^{-1} M) was prepared from $K_2Cr_2O_7$ in Milli-Q water. The solution was diluted to 10^{-4} M of Cr(VI). The pH of the initial working solution was 6.9.

2.2. Catalyst preparation

Copper sulfide nanostructures (CuS NSs) were prepared according to Pal et al. (2015) by using $CuCl_2$ as copper precur-

sor, thiourea as sulfur precursor and triethanolamine as a complexing agent. Briefly, a mixture of 15 mL of $CuCl_2$ (0.5 M), 5 mL of TEA, 10 mL of NH_4OH, 10 mL of NaOH (1 M), 15 mL of thiourea (0.5 M), and 45 mL of deionized water was heated at 50 °C for 1 h under magnetic stirring, after which a precipitate was formed. The formed precipitate was separated by centrifugation, rinsed with Milli-Q water, ethanol, and then dried overnight at room temperature to give approximately 800 mg of CuS NSs as a dark greenish powder.

Highly crystalline pure covellite (CuS) phase was prepared by hydrothermal method. Briefly, 160 mg (32 mM) of $CuSO_4 \cdot 5H_2O$ and 100 mg (32 mM) of NaS_2O_3 were dissolved in 20 mL of water and sonicated (35 kHz) for 2 h. The solution was then transferred into a Teflon-lined stainless steel autoclave (40 mL capacity) and kept at 90 °C for 24 h. Then the autoclave was cooled to ambient temperature. The resulting precipitate was washed repeatedly with deionized water and ethanol, and finally dried at 40 °C for 4 h.

2.3. Photocatalytic reduction of Cr(VI)

The visible light photocatalytic reduction of Cr(VI) was performed in a 1 cm spectrometric quartz cuvette at room temperature. In short, a 2 mL aqueous solution of Cr(VI) (10^{-4} M) and CuS NSs was irradiated under stirring at $\lambda > 420$ nm (0.41 W) using a visible fiber lamp (Spot Light Source 400–700 nm, L9566-03, Hamamatsu, Japan). The performance of the CuS NSs photocatalyst was assessed by monitoring the decay of the characteristic absorption band of Cr(VI) at 352 nm as a function of irradiation time. All experiments were realized in triplicate.

The visible light photocatalytic performance of CuS NSs for Cr(VI) reduction in presence of formic or adipic acid was carried out by addition of 100 µL of 10^{-1}, 10^{-2} or 10^{-3} M of the acid into 1 cm spectrometric quartz cuvette containing 2 mL aqueous solution of $K_2Cr_2O_7$ (10^{-4} M).

2.4. Photocatalytic reduction of Cr(VI) in simulated water

To check the practical applicability of CuS NSs, a water from a local lake (lac du Héron, Villeneuve d'Ascq, France) was used to dissolve $K_2Cr_2O_7$. The visible light ($\lambda > 420$ nm) photo-reduction of 10^{-4} M Cr(VI) was examined in absence and presence of adipic acid (0.5 or 1 mM) at room temperature. The reduction process was assessed by the decay of the characteristic absorption band of Cr(VI) at 352 nm using UV–vis spectrometry. All experiments were realized in triplicate.

2.5. Characterization

The CuS NSs crystal phase was analyzed by X-ray diffraction (XRD) at room temperature using Rigaku Smartlab rotated anode diffractometer, equipped with a copper anode Cu Kα radiation (λ = 1.5406 Å) and P = 9 kW. The 2θ ranged from 15° to 80° and the scanning speed was 0.5°/min at a step of 0.01°.

The CuS NSs morphology was examined using scanning electron microscopy (ULTRA 55, Zeiss) equipped with an X-ray energy dispersive analysis device (EDX analysis) (Bruket AXS), and transmission electron microscopy (Philips CM30 microscope operating at 300 kV). The microscope was equipped with a Gatan SS CCD camera and a Digital Micrograph software for the acquisition of electron diffraction patterns, bright field and high-resolution imaging.

The optical properties of CuS NSs were recorded using a Perkin Elmer Lambda UV–Vis 950 spectrophotometer equipped with an Angle Absolute Universal Reflectance Accessory (URA).

The chemical composition of CuS NSs was analyzed using X-ray photoelectron spectroscopy (XPS) (ESCALAB 220 XL spectrometer from Vacuum Generators featuring a monochromatic Al Kα X-ray source at 1486.6 eV).

3. Results and discussion

The CuS NSs were synthesized according to Pal et al. (2015). Their crystalline phase was examined by X-ray diffraction (XRD). Fig. 1 depicts the XRD pattern of the as-prepared CuS NSs. It comprises peaks at 2θ values of 27.89°, 29.26°, 31.93°, 33.26°, and 48.08° due to diffraction of the (1 0 1), (1 0 2), (1 0 3), (0 0 6), and (1 1 0) planes, respectively; the minor peaks at 2θ values of 38.95°, 42.2°, 52.59°, and 59.2° could be indexed to (1 0 5), (1 0 6), (1 0 8), and (1 1 6) planes, respectively. All the diffraction peaks could be readily indexed to the hexagonal phase of CuS (JCPDS No. 06-0464), in good agreement with reported data (Meng et al., 2013, Pal et al., 2015). It is worth to notice the presence of small diffraction peaks at 22.78°, 35.63°, 36.50°, 39.76°, 41.28°, and 61.58° due to $Cu_4SO_4(OH)_6$. Halder-Wagner method (Halder and Wagner, 1966) was used to study the individual contributions of the crystallite size and lattice micro-strain to isotropic line broadening of all the reflection peaks of CuS NSs, as implemented in the PDXL2 software (2012). It follows a value of crystallite size of 7 nm with a negligible microstrain contribution.

The morphology of the synthesized CuS NSs was investigated by scanning electron microscopy (SEM), transmission electron microscopy (TEM) and selected area electron diffraction (SAED). SEM imaging indicates the formation of particles in aggregated form with a flower-like geometry (Fig. 2). Fig. 3a,b exhibits typical TEM images of the CuS NSs showing

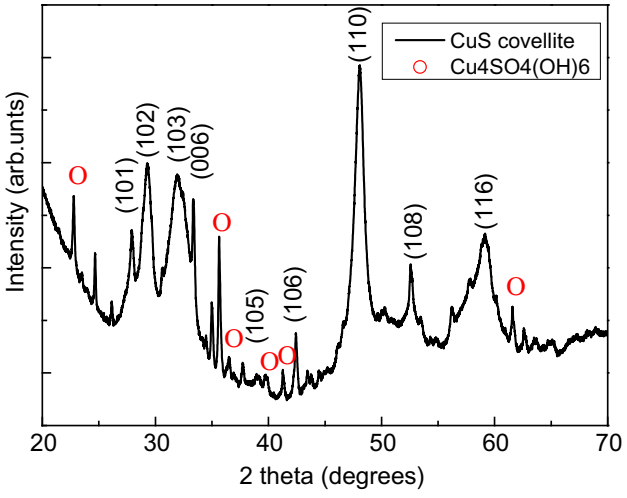

Fig. 1 X-ray diffraction pattern of as-prepared CuS NSs.

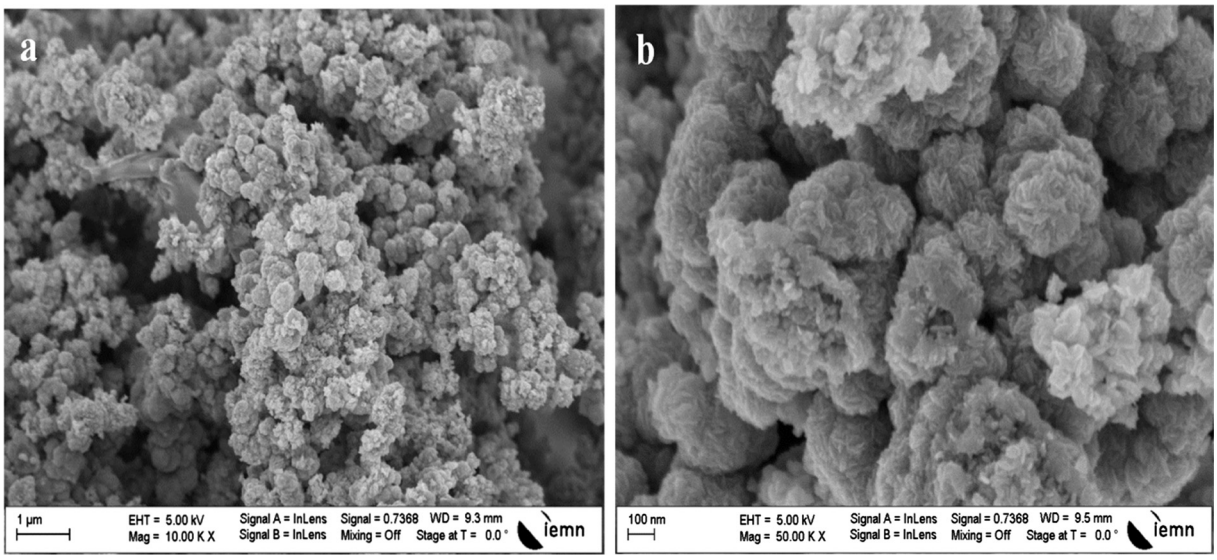

Fig. 2 Scanning electron microscopy (SEM) images of as-prepared CuS NSs.

sheet-like structures of about 50 nm in size. From the corresponding high resolution TEM image (Fig. 3c), a lattice interplanar spacing of 3.04 Å is measured, which is consistent with the d spacing for the (1 0 2) crystal plane of hexagonal phase of CuS (Meng et al., 2013). The selected area electron diffraction (SAED) pattern reveals the polycrystalline nature of as-prepared CuS NSs (Fig. 3d). The results are in good agreement with XRD analysis.

The optical properties of CuS NSs were studied by using UV–Vis spectrophotometry. It is worth to notice that CuS NSs absorption occurs in the visible light region, which makes the material a promising photocatalyst. The UV–vis spectrum of CuS NSs (Fig. 4a) exhibits a maximum absorption at ~ 450 nm and an extended absorption in the near infrared (NIR) region, characteristic of CuS covellite (Jia et al., 2013). From the plot of $(\alpha_{KM}h\nu)^2$ *versus hv* (where, α_{KM} is the absorption coefficient obtained from equation 1 using Kubelka-Munk formalism (Jia et al., 2013) and *hv* is the photon energy), the optical band gap E_g of CuS NSs was determined using the Tauc plot method (Fig. 4b):

$$\alpha_{KM} = (1 - R_\infty)^2 / 2R_\infty \quad (1)$$

where R_∞ is the reflectance of an infinitely thick sample with respect to a reference at each wavelength.

The optical gap is extracted from the x-intercept of the extension of the linear part of the plot $(\alpha_{KM}\ h\nu)^2$ *versus hv* (Zbao and Fendler, 1991). According to Tauc, the photon energy dependence of the absorption coefficient 'α_{KM}' can be described by the following Eq. (2):

$$\alpha_{KM}(h\nu) = A\,(h\nu - E_g)^n \quad (2)$$

where A is a constant, E_g the optical band, α_{KM} is the optical absorption coefficient, *hv* is the photon energy gap, h the Plank's constant and the exponent n is characteristic of the nature of the electron transition.

The exponent n depends on the type of band gap of the semiconductor and for a direct gap n = 1/2; thus the plot of $(\alpha_{KM}h\nu)^2$ *versus hv* is linear over a certain energy range and the intercept with the x-axis is precisely the value of the optical gap. For indirect band gap n = 2; in this case, $(\alpha_{KM}h\nu)^{1/2}$ is plotted *versus* (hν) and the value of the gap is determined similarly from the x-intercept. Assuming a direct transition, the relation (2) becomes:

$$(\alpha_{KM}h\nu)^2 = A\,(h\nu - E_g) \quad (3)$$

According to Eq. (3), a band gap of 2.07 eV was determined for the CuS NSs, in accordance with values reported for CuS NSs produced using a similar solution phase approach (Pal et al., 2015) or a hydrothermal route (Jia et al., 2013).

Furthermore, we have determined the potentials of the conduction band (CB) and valence band (VB) edges of CuS NSs using the well-known Mulliken electronegativity theory, by taking Cu_xS_y as an example (Mondal et al., 2015):

$$E_{CB} = X - E_e - \frac{1}{2}E_g;\ E_{VB} = E_{CB} + E_g$$

$$X = \{x_{Cu}^x \times x_S^y\}^{1/x+y}$$

$$X_{Cu} = \frac{1}{2}(A_{Cu} + I_{Cu}),$$

$$X_S = \frac{1}{2}(A_S + I_S),$$

where E_{CB} is the conduction band potential, X (5.27 eV for CuS) corresponds to the electronegativity of the semiconductor, E_e is the energy of free electrons on the hydrogen scale, which is 4.5 eV, E_g represents the band gap of the semiconductor (2.07 eV determined from the Tauc plot), A is the electron affinity energy, and I is the ionization energy.

Thus, from the Mulliken electronegativity equations, the top of the VB and the bottom of the CB of CuS NSs are estimated to be + 1.81 eV and −0.25 eV, respectively (Scheme 1).

The chemical composition of the synthesized CuS NSs was characterized using energy dispersive X-ray spectroscopy (EDS) and X-ray photoelectron spectroscopy (XPS). EDS analysis revealed atomic percentages of 55.91% and 44.09% for Cu and S, respectively (Fig. S1, Table S1). The result indi-

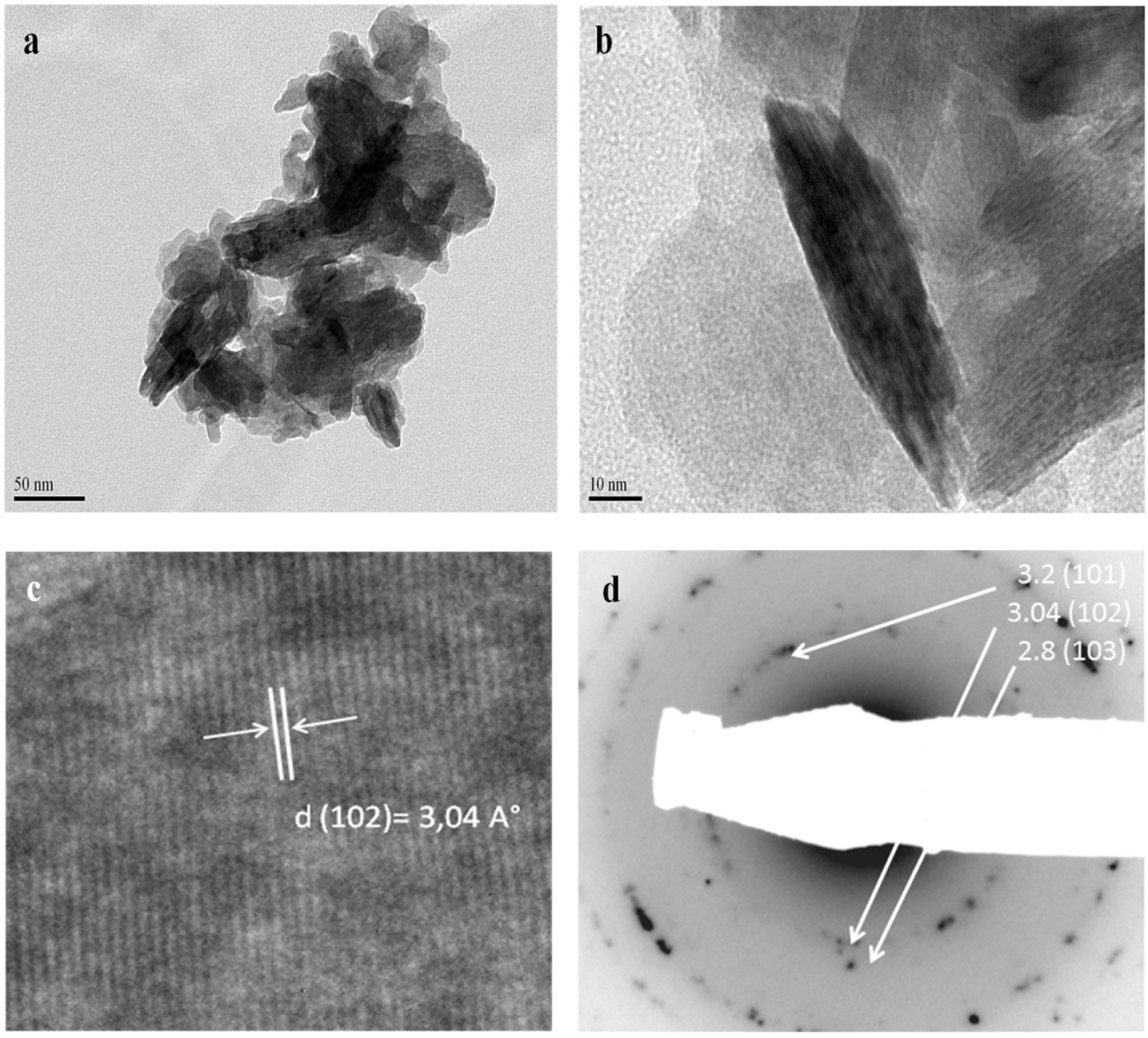

Fig. 3 (a and b) Typical TEM images, (c) HRTEM image showing lattice planes, and (d) selected area electron diffraction (SAED) pattern of CuS NSs, dotted pattern confirmed the crystalline nature of CuS NSs.

cates sulfur deficiency, which is characteristic of covellite phase. The other peaks in the EDS spectrum originate from the substrate used: Ni and C from the grid, Si and O from the detector.

The high resolution Cu_{2p} XPS spectrum of CuS NSs comprises two main peaks at 932.5 and 952.1 eV due to $Cu2p_{3/2}$ and $Cu2p_{1/2}$, respectively with an atomic percentage of 37.84% (Fig. 5a). The occurrence of a shakeup peak at 944.0 eV indicates the presence of Cu(II) species. The high resolution XPS spectrum of S_{2p} in Fig. 5b is characterized by a pair of peaks at 162.2 and 163.2 eV due to $S2p_{3/2}$ and $S2p_{1/2}$, respectively with an atomic percentage of 39.65% (Meng et al., 2013). The peak at 168.6 eV is most likely due to oxidized sulfur in the $Cu_4SO_4(OH)_6$. The atomic percentage ratio of Cu and S (Cu/S) is 0.95, close to a stoichiometric CuS material.

The Raman spectrum of the CuS NSs consists of a main peak at 469 cm^{-1} ascribed to S-S stretching vibration and a weaker peak at 264 cm^{-1} assigned to A_{1g} TO mode (Fig. S2), suggesting the formation of the covellite phase of CuS (Munce et al., 2007, Pal et al., 2015).

The visible light photocatalytic performance of the CuS NSs was evaluated for the Cr(VI) reduction to Cr(III) using UV–vis spectrophotometry. The progress of the photocatalytic process was assessed by recording the decrease of the characteristic absorption peak of Cr(VI) at ~352 nm over time (Fig. S3). The effect of the CuS NSs photocatalyst loading was investigated for the reduction of 10^{-4} M $K_2Cr_2O_7$ at room temperature (Fig. 6a). Increasing the mass loading from 1 to 3 mg had a significant effect on the reduction process with a photocatalyst loading of 3 mg exhibiting a full reduction after 60 min. This contrasts with a reduction efficiency of ~95% achieved using 1 and 2 mg of photocatalyst after 210 and 130 min irradiation, respectively. The result accounts for the presence of more active sites at higher photocatalyst dosage.

The Langmuir-Hinshelwood (L-H) kinetic model, initially developed to describe quantitatively gaseous–solid reactions, was recently employed to describe Cr(VI) photoreduction over

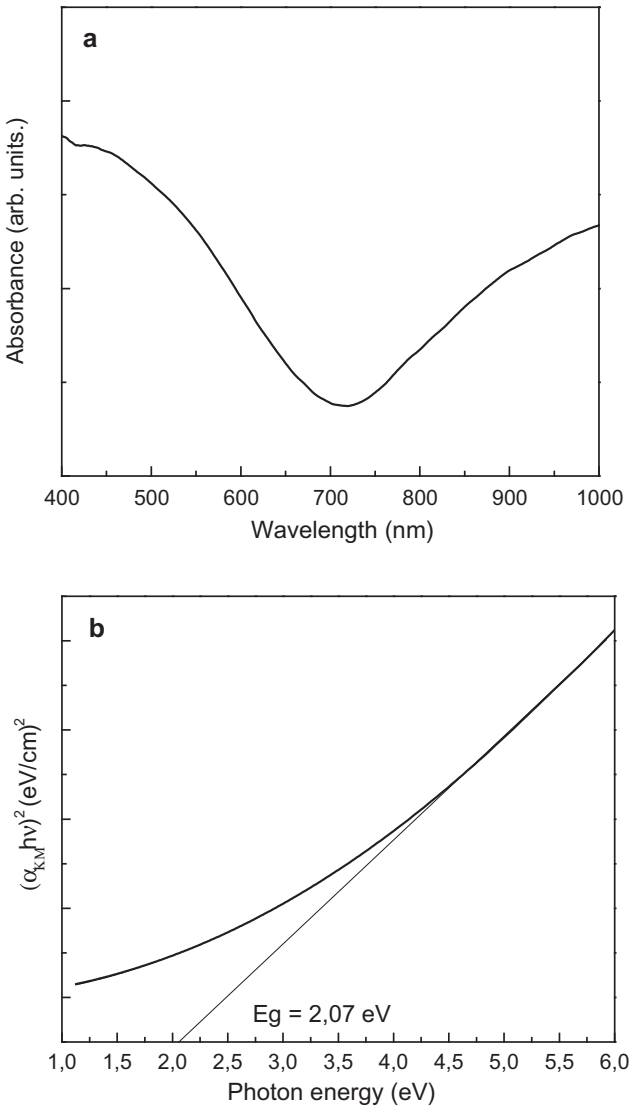

Fig. 4 (a) Optical absorption spectrum of CuS NSs (1 mg in 4 mL H_2O) and (b) plot of the square of absorbance $(\alpha_{KM}\ h\nu)^2$ *versus* photon energy hν.

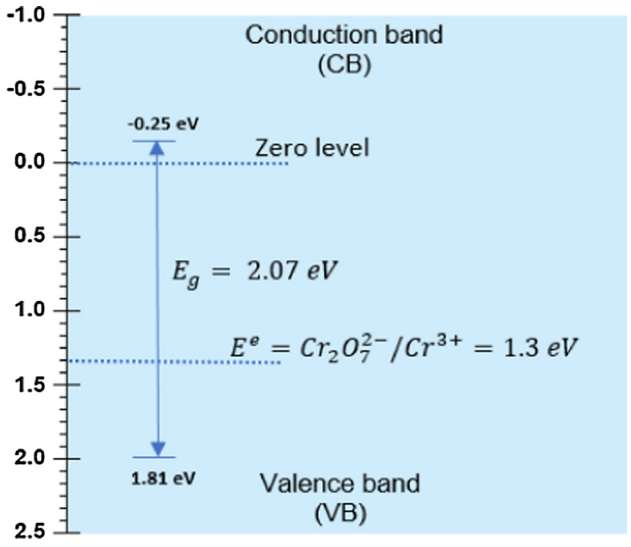

Scheme 1 Diagram of the energy band structure of CuS NSs.

metal oxide nanoparticles (Idris et al., 2011). In this model, the rate of reaction (r) is proportional to the fraction of surface covered by the substrate (θ). The rate of reaction (r) for low concentrations of substrate is given by:

$$r = -\frac{dC}{dt} = k_r\theta_r = \frac{k_r.KC}{(1+KC)} = k_{app}.C \quad (4)$$

For low Cr(VI) concentrations, the photoreduction of Cr(VI) follows pseudo-first order kinetics and the rate constant can be determined by the following relation (Idris et al., 2011):

$$-\ln\left(\frac{C}{C_0}\right) = k_{app}.t \quad (5)$$

where C_0 is the initial concentration of Cr(VI), C is the concentration of Cr(VI) at time *t*, *t* is the irradiation time and k_{app} is the rate constant (min^{-1}).

Using this model, the apparent pseudo first-order rate constant k_{app} is deduced from the slope of the line (Fig. 6b). A k_{app} value of 0.076 min^{-1} was obtained for CuS NSs loading of 3 mg, which is much higher than 0.017 min^{-1} determined for 1 mg (Table S2). This loading was used for further experiments.

Finally, the effect of organic acids (adipic or formic acid) on the visible light photoreduction of Cr(VI) using CuS NSs as photocatalyst was investigated. Fig. 7a depicts the influence of adipic acid concentration on the photoreduction of an aqueous solution of 10^{-4} M Cr(VI) in presence of 3 mg CuS NSs. The result clearly indicates that increasing the adipic acid concentration from 0.05 mM to 0.5 mM induced a significant decrease of the reduction time from 27 to 12 min, as compared to 60 min required for full Cr(VI) photoreduction in absence of adipic acid. The reaction kinetics can be fitted with a pseudo-first order model (Fig. 7b) and k_{app} values of 0.144 and 0.316 min^{-1} were obtained for 0.05 mM to 0.5 mM adipic acid, respectively (Table S3).

Similarly, the influence of formic acid on the photocatalytic reduction of Cr(VI) using CuS NSs as photocatalyst was examined. Fig. 8a displays the influence of formic acid concentration on the photoreduction of a 10^{-4} M Cr(VI) aqueous solution in the presence of 3 mg of CuS NSs. Although addition of formic acid at 0.5 mM led to a significant reduction of the photocatalytic time to 25 min to achieve full reduction of Cr(VI), the effect was less important than that observed upon addition of adipic acid. It is worth noting that the pH of the solution was not the main reason for this difference in the reduction rate. Indeed, comparable pH values have been reached upon addition of adipic acid or formic acid. By fitting the data with a pseudo-first order model (Fig. 8b), k_{app} values of 0.101 and 0.248 min^{-1} were recorded for 0.05 mM to 0.5 mM formic acid, respectively (Table S4).

In a control experiment, we have examined the effect of formic acid on the Cr(VI) reduction in absence of CuS NSs. The results showed that, under dark conditions and in absence of CuS NSs, no reduction occurred upon addition of 0.5 mM formic acid to 10^{-4} M Cr(VI) aqueous solution even after 60 min exposure at room temperature (Fig. S4). The result clearly suggests that the presence of CuS NSs photocatalyst was mandatory to achieve Cr(VI) reduction.

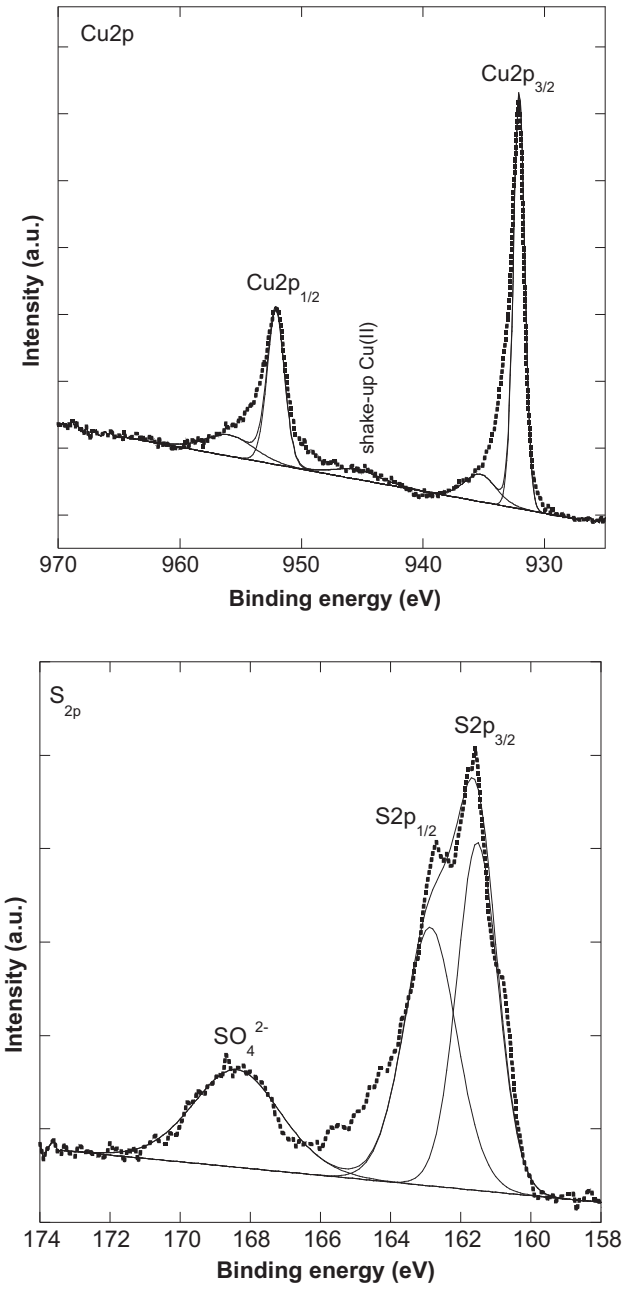

Fig. 5 (a) Cu_{2p} and (b) S_{2p} high resolution X-ray photoelectron spectroscopy (XPS) of CuS NSs.

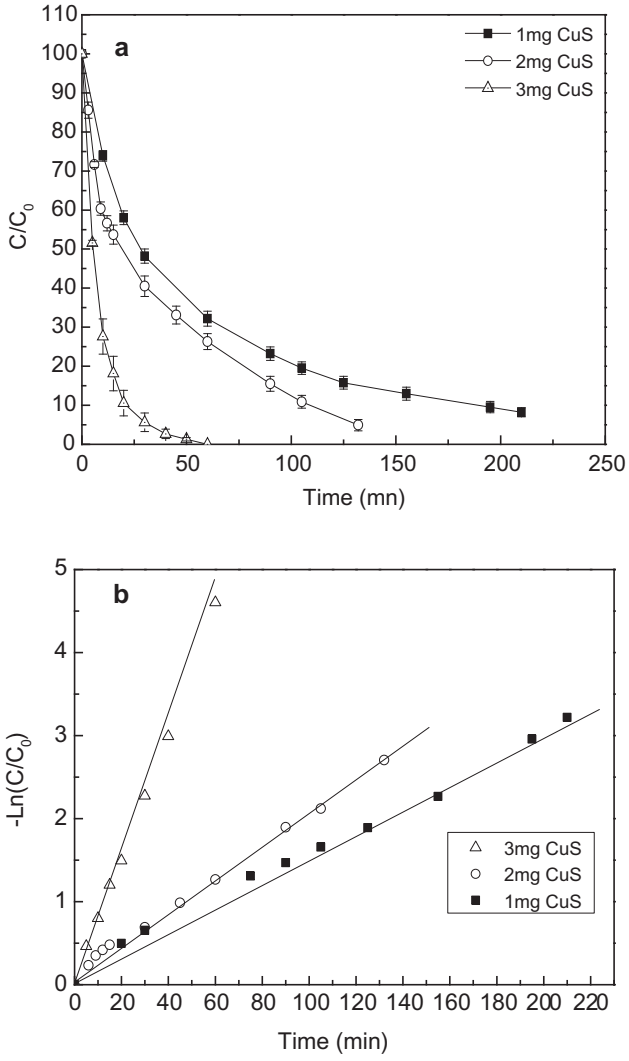

Fig. 6 Photocatalytic reduction of 10^{-4} M $K_2Cr_2O_7$ aqueous solution in the presence of CuS NSs (1, 2 and 3 mg) under visible light irradiation (a) and the corresponding degradation kinetics with first order linearity of $-\ln(C/C_0) = kt$ (b).

To study the influence of the $Cu_4SO_4(OH)_6$ phase on the photocatalytic reduction of Cr(VI), we have prepared a pure phase of CuS through a hydrothermal process (see experimental part). XRD diffraction pattern of the prepared CuS clearly shows the formation of the highly crystalline phase pure covellite (Fig. S5). The peaks at 2θ values of 27.57°, 29.24°, 31.75°, 32.86°, 47.92°, 52.67°, and 59.22° could be indexed to the (1 0 1), (1 0 2), (1 0 3), (0 0 6), (1 1 0), (1 0 8), and (1 1 6) planes, respectively.

The pure CuS phase was then investigated for the photoreduction of Cr(VI) under otherwise identical experimental conditions (Fig. S6). The pure CuS phase is slightly more active than the CuS NSs for the low catalyst loadings (1 and 2 mg) and almost comparable for a catalyst loading of 3 mg. The results clearly indicate that the $Cu_4SO_4(OH)_6$ phase does not influence the photocatalytic reduction of C(VI). The slightly lower activity of CuS NSs compared to pure CuS may be attributed to the difference in the content of active CuS phase in both catalysts.

The photocatalytic activity of Cu NSs was further tested using simulated water (water from a local lake, Fig. 9a). $K_2Cr_2O_7$ was dissolved at an initial concentration of 10^{-4} M and irradiated using visible light. As can be seen in Fig. 9b, in absence of adipic acid, a saturation was attained after 30 min irradiation with 60% reduction of Cr(VI). Further irradiation did not improve the photocatalytic reduction process. Addition of 0.5 mM adipic acid improved slightly the photocatalytic process with a total Cr(VI) removal of 72% after 30 min irradiation, and reached 80% after 240 min. Increasing adipic acid concentration to 1 mM accelerated significantly the reduction rate of Cr(VI), reaching 100% after 50 min irradiation. The results are in accordance with those obtained using

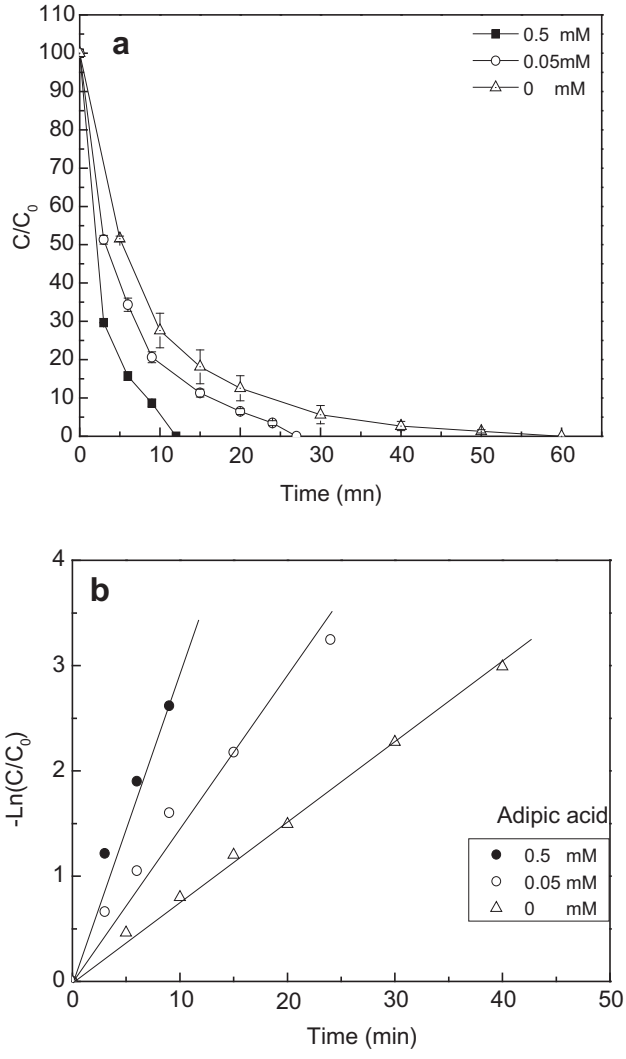

Fig. 7 Photocatalytic reduction of 10^{-4} M $K_2Cr_2O_7$ aqueous solution using 3 mg of CuS NSs in the presence of adipic acid 0 mM (pH = 6.9), 0.05 mM (pH = 6.3) and 0.5 mM (pH = 4.5) under visible light irradiation (a) and the corresponding degradation kinetics with first order linearity of $-\ln(C/C_0) = kt$ (b).

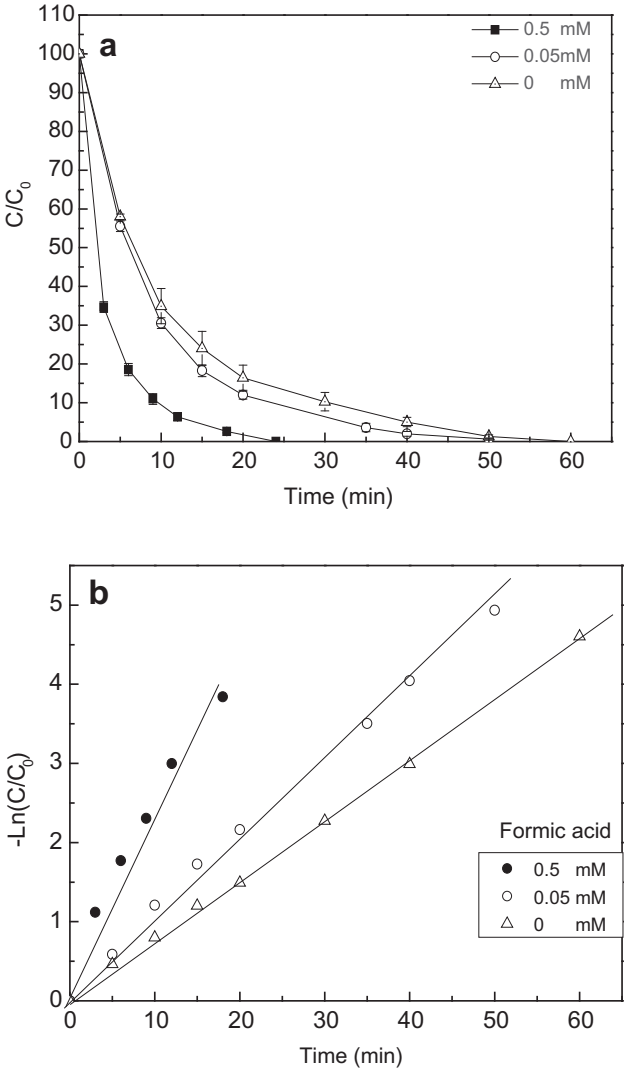

Fig. 8 Photocatalytic reduction of 10^{-4} M $K_2Cr_2O_7$ aqueous solution using 3 mg of CuS NSs in the presence of formic acid 0 mM (pH = 6.9), 0.05 mM (pH = 6.16) and 0.5 mM (pH = 4.12) under visible light irradiation (a) and the corresponding degradation kinetics with first order linearity of $-\ln(C/C_0) = kt$ (b).

Milli-Q water for dissolving Cr(VI), indicating the positive effect of adipic acid on the photocatalytic process.

The stability of the photocatalyst was investigated by recording seven consecutive photoreduction runs of a 10^{-4} M Cr(VI) aqueous solution in presence of 1 mg of pure CuS phase and 0.1 mM adipic acid under visible light irradiation (Fig. S7). The photocatalyst exhibited a good stability in the first 4 cycles with full Cr(VI) reduction to Cr(III) after 8 min visible light irradiation. However, the reduction time increased thereafter to reach 16, 24 and 60 min to achieve full reduction after the 5th, 6th and 7th cycle, respectively.

The deactivation of the CuS photocatalyst after the 4th cycle is most likely due to Cr(III) adsorption on the surface of the photocatalyst. Indeed, XPS analysis of the sample after photocatalysis indicates the presence of Cr on the surface. More interestingly, the Cr_{2p} high resolution XPS spectrum (Fig. S6) consists of reduced forms of Cr namely Cr(III). The binding energies at 577.2 and 587.4 eV assigned to $Cr2p_{3/2}$ and $Cr2p_{1/2}$, respectively confirm that the adsorbed Cr is in the form of Cr(III). Cr(VI) is generally characterized by higher binding energies at around 580 and 589 eV for $Cr2p_{3/2}$ and $Cr2p_{1/2}$, respectively (Park et al., 2008).

A plausible mechanism can be proposed based on the optical characteristics of the CuS photocatalyst. With an optical band gap of 2.07 eV, CuS absorbs visible light to generate an electron-hole pair (Eq. (6)). Reaction of the photoexcited hole with surface adsorbed H_2O molecule on the photocatalyst surface leads to the formation of $HO^{\cdot}$ radicals (Eq. (8)). A re-oxidation of Cr(III) to Cr(VI) is possible upon reaction of Cr(III) with holes and $HO^{\cdot}$ (Eq. (9)).

$$CuS + h\nu \rightarrow h^{+}_{VB} + e^{-}_{CB} \quad (6)$$

$$Cr_2O_7^{2-} + 14H^{+} + 6e^{-} \rightarrow 2Cr^{3+} + 7H_2O \quad (7)$$

$$H_2O + h^{+} \rightarrow HO^{\cdot} + H^{+} \quad (8)$$

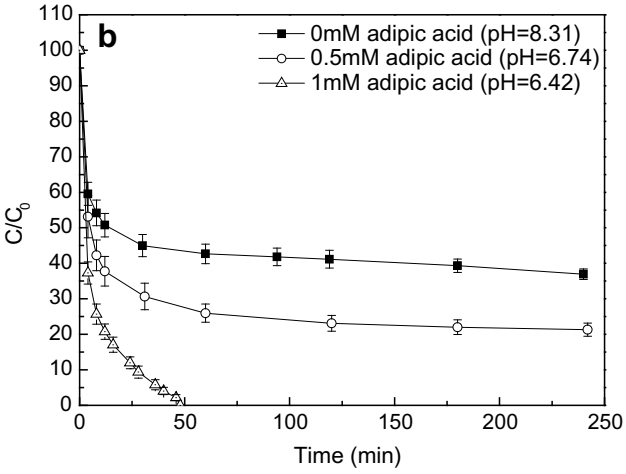

Fig. 9 Photo of the lake (a); Photocatalytic reduction of 10^{-4} M $K_2Cr_2O_7$ dissolved in water from a local lake using 3 mg of CuS NSs in the presence of adipic acid 0 mM (pH = 8.31), 0.5 mM (pH = 6.74) and 1 mM (pH = 6.42) under visible light irradiation (b).

$$Cr^{3+} + 2h^{+} + HO^{\cdot} \rightarrow Cr^{6+} + HO^{-} \quad (9)$$

$$HO^{\cdot} + \text{organic acid} \rightarrow \ldots \rightarrow CO_2 + H_2O \quad (10)$$

$$h^{+} + \text{organic acid} \rightarrow \ldots \rightarrow CO_2 + H_2O \quad (11)$$

Although Cr(VI) reduction was promoted by CuS NSs alone under visible light irradiation, addition of organic acids enhanced the reduction rate. Organic acids are suspected to scavenge the photogenerated holes directly (Eq. (11)) or indirectly through the reaction with $HO^{\cdot}$ (Eq. (10)), generated by reaction with adsorbed water molecules (Eq. (8)). In both cases, hole consumption prevents electron-hole recombination therefore enhances Cr(VI) reduction (Eq. (7)). The difference in the efficiency of the two investigated organic acids i.e. adipic acid and formic acid is related to their electronic/structural properties (Fellahi et al., 2016, Prairie et al., 1999). It has been suggested that organic acids able to transfer electrons directly to the photocatalyst valence band are more efficient than those that are oxidized only by $HO^{\cdot}$ radicals. In the former case, electron-hole recombination is minimized because electrons

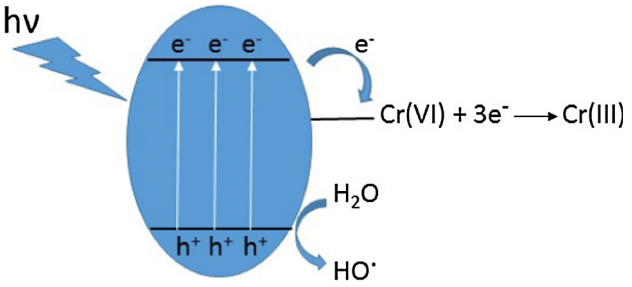

Scheme 2 Plausible mechanism of Cr(VI) reduction using CuS NSs photocatalyst under visible light irradiation.

generated from the organic acid will fill rapidly valence band holes, making more conduction band electrons available for Cr(VI) reduction (Eq. (7)). For organic acids reacting with $HO^{\cdot}$ radicals (Eq. (10)), Cr(VI) reduction is indirectly affected; the holes are only filled by the formation of $HO^{\cdot}$ radicals, leading to a slow photoreduction rate.

Additionally, we studied the effect of O_2 and H_2O_2 on the photocatalytic reduction of Cr(VI) under visible light irradiation (Fig. S9). The role of oxygen on the photocatalytic reduction of Cr(VI) was pointed out previously (Hu et al., 2014). Indeed, it was suggested that O_2 can capture the conduction band electrons to generate $O_2^{\cdot-}$ (Eq. (12)) able to reduce Cr (VI) to Cr(V) (Eq. (13)). To illustrate the effect of O_2 on the photoreduction of Cr(VI), the solution was degassed with N_2 (Fig. S9). The results indicate that the Cr(VI) reduction is slightly lower in absence of O_2, suggesting that $O_2^{\cdot-}$ is not the dominant species in the photocatalytic process. Similarly, H_2O_2 alone (in absence of CuS NSs) was not efficient for the reduction of Cr(VI) either in the dark or under photoillumination (Fig. S9). In the presence of CuS NSs, H_2O_2 had a negligible effect in the dark, while the Cr(VI) photoreduction was slightly enhanced under visible light irradiation. The results indicate that H_2O_2 contribution in the Cr(VI) reduction is not significant.

$$O_2 + e^{-} \rightarrow O_2^{\cdot-} \quad (12)$$

$$Cr(VI) + O_2^{\cdot-} \rightarrow Cr(V) + O_2 \quad (13)$$

Taken together, Cr(VI) reduction is believed to occur dominantly according to Scheme 2.

4. Conclusion

We have successfully applied CuS nanostructures, synthesized by a wet chemical approach, as an efficient visible light photocatalyst for Cr(VI) reduction to Cr(III). The photocatalytic efficiency was enhanced by addition of adipic acid or formic acid. The results indicated that the electronic and structural characteristics of these organic compounds are important factors for Cr(VI) photoreduction. Under optimized conditions, addition of adipic acid led to full Cr(VI) reduction within only 12 min at room temperature, as compared to 60 min that are necessary to attain the same reduction degree using CuS NSs alone. While these organic species are believed to act as hole scavengers thus improving charge separation in the photocatalytic process, the difference in their impact on the reduction rate is not very clear. The efficacy of CuS NSs or the photore-

duction of Cr(VI) dissolved in water from a local lake was further demonstrated. Future work will focus on hybridization of the CuS nanostructures with carbon supports such as carbon dots or graphene with the aim to improve the charge separation and increase their absorption in the visible range.

Acknowledgements

The authors gratefully acknowledge financial support from the Centre National de la Recherche Scientifique (CNRS), the University of Lille, the Hauts-de-France region. Sawsen Nezar acknowledges financial support from the Ministry of High Education and Scientific Research of Algeria for 11-month fellowship.

Conflict of interest

The authors declare that they have no conflict of interest.

Appendix A. Supplementary material

Supplementary data associated with this article can be found, in the online version, at https://doi.org/10.1016/j.arabjc.2018.01.002.

References

Barrera-Díaz, C.E., Lugo-Lugo, V., Bilyeu, B., 2012. J. Hazard. Mater. 223–224, 1–12.
Celebi, M., Yurderi, M., Bulut, A., Kaya, M., Zahmakiran, M., 2016. Appl. Catal. B: Environm. 180, 53–64.
Dandapat, A., Jana, D., De, G., 2011. Appl. Catal. A: General 396, 34–39.
Deng, B., Stone, A., 1996. Environ. Sci. Technol. 30, 2484–2494.
Depault, F., Cojocaru, M., Fortin, F., Chakrabarti, S., Lemieux, N., 2006. Toxicol. in Vitro 20, 513–518.
Estrada, A.C., Silva, F.M., Soares, S.F., Coutinho, J.A.P., Trindade, T., 2016. RSC Adv. 6, 34521–34528.
Fellahi, O., Barras, A., Pan, G.-H., Coffinier, Y., Hadjersi, T., Maamache, M., Szunerits, S., Boukherroub, R., 2016. J. Hazard. Mater. 304, 441–447.
Gheju, M., 2011. Water Air Soil Pollut. 222, 103–148.
Goel, S., Chen, F., Cai, W., 2014. Small 10, 631–645.
Gupta, V.K., Pathania, D., Agarwal, S., Singh, P., 2012. J. Hazard. Mater. 243, 179–186.
Hai, Z., Huang, J., Remita, H., Chen, J., 2013. Mater. Lett. 108, 304–307.
Halder, N.C., Wagner, N.C.J., 1966. Acta Crystallogr. 20, 312–313.
Hu, X.-S., Shen, Y., Xu, L.-H., Wang, L.-M., Xing, Y.-J., 2016. J. Alloys Compds. 674, 289–294.
Hu, X., Ji, H., Chang, F., Luo, Y., 2014. Catal. Today 224, 34–40.
Idris, A., Hassan, N., Rashid, R., Ngomsik, A.-F., 2011. J. Hazard. Mater. 186, 629–635.
Jia, B., Qin, M., Jiang, X., Zhang, Z., Zhang, L., Liu, Y., Qu, X., 2013. J. Nanopart. Res. 15, 1469.
Jin, W., Du, H., Zheng, S., Zhang, Y., 2016. Electrochim. Acta 191, 1044–1055.
Marinho, B.A., Cristóvão, R.O., Loureiro, J.M., Boaventura, R.A.R., Vilar, V.J.P., 2016. Appl. Catal. B: Environm. 192, 208–219.
Meng, X., Tian, G., Chen, Y., Zhai, R., Zhou, J., Shi, Y., Cao, X., Zhou, W., Fu, H., 2013. CrystEngComm 15, 5144–5149.
Mondal, C., Singh, A., Sahoo, R., Sasmal, A.K., Negishi, Y., Pal, T., 2015. New J. Chem. 39, 5628–5635.
Munce, C.G., Parker, G.K., Holt, S.A., Hope, G.A., 2007. Colloids Surf. A: Physicochem. Eng. Aspects 295, 152–158.
Omole, M.A., K'owino, I.O., Sadik, O.A., 2007. Appl. Catal. B: Environ. 76, 158–167.
Owlad, M., Aroua, M.K., Daud, W.A.W., Baroutian, S., 2009. Water Air Soil Pollut. 200, 59–77.
Pal, M., Mathews, N.R., Sanchez-Mora, E., Pal, U., Paraguay-Delgado, F., Mathew, X., 2015. J. Nanopart. Res. 17, 301.
Park, D., Yun, Y.-S., Park, J.M., 2008. J. Colloid Interface Sci. 317, 54–61.
PDXL2, 2012. Advanced integrated X ray powder diffraction suite. Rigaku J. 28, 29–30.
Prairie, M.R., Evans, L.R., Stange, B.M., Marlinez, S.L., 1999. Environ. Sci. Technol. 27, 1776–1782.
Saranya, M., Ramachandran, R., Samuel, E.J.J., Jeong, S.K., Grace, A.N., 2015. Powder Technol. 279, 209–220.
Sen, M., Ghosh Dastidar, M., 2010. Iran. J. Environ. Health. Sci. Eng. 7, 182–190.
Srinivas, B., Kumar, B.G., Muralidharan, K., 2015. J. Mol. Catal. A: Chem. 410, 8–18.
Van Der Stam, W., Berends, A.C., De Mello Donega, C., 2016. ChemPhysChem 17, 559–581.
Voitkun, V., Zhitkovich, A., Costa, M., 1998. Nucl. Acids Res. 26, 2024–2030.
Wang, H., Ren, Z.J., 2014. Water Res. 66, 219–232.
Wang, J., Liang, Y., Jin, Q., Hou, J., Liu, B., Li, X., Chen, W., Hayat, T., Alsaedi, A., Wang, X., 2017a. ACS Sustain. Chem. Eng. 5, 5550–5561.
Wang, J., Wang, P., Wang, H., Dong, J., Chen, W., Wang, X., Wang, S., Hayat, T., Alsaedi, A., Wang, X., 2017b. ACS Sustain. Chem. Eng. 5, 7165–7174.
Wen, T., Fan, Q., Tan, X., Chen, Y., Chen, C., Xu, A., Wang, X., 2016. Polym. Chem. 7, 785–794.
Wen, T., Wang, J., Yu, S., Chen, Z., Hayat, T., Wang, X., 2017. ACS Sustain. Chem. Eng. 5, 4371–4380.
Zbao, X.K., Fendler, J.H., 1991. J. Phys. Chem. 95, 3716–3723.
Zhao, Y., Burda, C., 2012. Energy Environ. Sci. 5, 5564–5576.